Functional characterisation and subcellular localisation of HCN1 channels in rabbit retinal rod photoreceptors

Gian Carlo Demontis*, Anna Moroni†, Biagio Gravante†, Claudia Altomare†, Biancamaria Longoni‡, Luigi Cervetto* and Dario DiFrancesco†§

Dipartimento di Psichiatria, Neurobiologia, Farmacologia e Biotecnologie, Università di Pisa, Via Bonanno, 6-56126 Pisa, †Dipartimento di Fisiologia e Biochimica Generali, Laboratorio Fisiologia Molecolare e Neurobiologia, Università di Milano, Milan, ‡Dipartimento di Neuroscienze, Università di Pisa, Via Roma, 33-56126 Pisa and §INFM, Università di Milano, Via Celoria, 26-20133 Milan, Italy

Gating of voltage-dependent conductances in retinal photoreceptors is the first step of a process leading to the enhancement of the temporal performance of the visual system. The molecular components underlying voltage-dependent gating in rods are presently poorly defined. In the present work we have investigated the isoform composition and the functional characteristics of hyperpolarisation-activated cyclic nucleotide-gated channels (HCN) in rabbit rods. Using immunocytochemistry we show the expression in the inner segment and cell body of the isoform 1 (HCN1). Electrophysiological investigations show that hyperpolarisation-activated currents (I_h) can be measured only from the cell regions where HCN1 is expressed. Half-activation voltage (-75.0 ± 0.3 mV) and kinetics ($t_{1/2}$ of 101 ± 8 ms at -110 mV and 20 °C) of the I_h in rods are similar to those of the macroscopic current carried by homomeric rabbit HCN1 channels expressed in HEK 293 cells. The homomeric nature of HCN1 channels in rods is compatible with the observation that cAMP induces a small shift (2.3 ± 0.8 mV) in the half-activation voltage of I_h. In addition, the observation that within the physiological range of membrane potentials, cAMP does not significantly affect the gain of the current-to-voltage conversion, may reflect the need to protect the first step in the processing of visual signals from changes in cAMP turnover.

The tight packing of rhodopsin in the outer segment of retinal rod photoreceptors optimises the quantum catch but limits the speed of phototransduction (Calvert *et al.* 2001). There is evidence to suggest that signal processing taking place at early retinal stages in mammals compensates for the slow kinetics of the transductive cascade (Gargini *et al.* 1999*a*). Hyperpolarisation-activated currents (I_h) have been shown to play a relevant role in improving the temporal performance of visual signals at the level of rods (Demontis *et al.* 1999) and/or bipolar cells (Gargini *et al.* 1999*b*). I_h and its cardiac counterpart I_f (reviewed by DiFrancesco, 1993; Pape, 1996) are carried through hyperpolarisation-activated and cyclic-nucleotide-gated channels (HCN), which are characterised by six membrane-spanning domains and one cyclic nucleotide-binding domain (CNBD) in the long carboxy-terminal tail (Santoro *et al.* 1997). Binding of cAMP allosterically modulates voltage-dependent gating (DiFrancesco, 1999; Wainger *et al.* 2001), thus raising the possibility that changes in cAMP turnover modulate the temporal resolution of rod-mediated vision via a control of I_h gating in rods and/or bipolar cells. This possibility critically depends on the isoform composition of HCN channels. In recent years several isoforms (HCN1 to 4) have been identified (Gauss *et al.* 1998; Ludwig *et al.* 1998; Santoro *et al.* 1998; Ludwig *et al.* 1999; Seifert *et al.* 1999) and homomeric channels composed of different isoforms with distinct kinetics and cAMP sensitivity have been characterised. HCN1 channels, for example, have the fastest kinetics and the lowest sensitivity to cAMP (Ludwig *et al.* 1998; Santoro *et al.* 1998), compared to HCN2 and HCN4, which have similarly substantial cAMP sensitivity (Ludwig *et al.* 1999; Seifert *et al.* 1999; Moroni *et al.* 2000). Additional complexity is provided by the coexpression in neurones and in cardiac cells of multiple HCN isoforms (Moosmang *et al.* 1999; Franz *et al.* 2000; Santoro *et al.* 2000; Moroni *et al.* 2001), which may associate to form heteromeric channels with kinetics and cAMP sensitivity distinct from those of homomeric channels (Chen *et al.* 2001; Ulens & Tytgat, 2001).

The isoform composition of HCN in rods has been addressed by Moosmang *et al.* (2001) using *in situ* hybridisation with riboprobes. Their conclusion that HCN1 is the only isoform expressed by photoreceptors is not supported by kinetic measurements and/or immunocytochemical localisation. Moreover, a recent report by Muller *et al.* (2001) suggests that isoforms distinct from HCN1 are expressed in photoreceptors.

In the present paper we show that both HCN1 mRNA and protein are expressed in the rabbit retina. By confocal image analysis of rabbit rods immunolabelled with an antibody against rabbit HCN1 we were able to show that HCN1 protein is localised in selected compartments of the rod. Furthermore, by means of perforated-patch recordings we show that the kinetics and cAMP-induced shift of the activation curve are consistent with those of homomeric HCN1 channels expressed in heterologous systems. Our data show that in the range of membrane potentials of physiological relevance for mammalian rods, the gain of the current-to-voltage conversion is not affected by cAMP.

METHODS

Tissue preparation

New Zealand albino rabbits weighing 0.8–1 kg were anaesthetised by intra-muscular injection of xylazine (4.6 mg kg^{-1}) and ketamine (60 mg kg^{-1}) and killed by cervical dislocation after loss of corneal reflexes. The investigation conformed with guidelines for the care and use of laboratory animals as established by State (D. L. 116/1992) and European directives (86/609/CEE) as well as those of the US National Institutes of Health (NIH Publication No. 85-23, revised 1996). Animal research authorisation was granted by the Department of Food, Nutrition and Public Veterinary Health of the Italian Ministry of Health.

The eyes were quickly enucleated in normal room light. Each eye was hemisected just behind the ora serrata, the vitreous carefully removed and the retina isolated from the sclera. The retina was stored frozen at −70 °C until used for Northern and Western blot analysis. For immunolocalisation and electrophysiological investigation the retina was put in a dish with cold Tyrode solution and allowed to recover before enzymatic treatment. It was then incubated for 25–35 min at 37 °C with 1 mg ml^{-1} papain (17 U mg^{-1}, Sigma-Aldrich s.r.l., Italy) activated by 0.3 mg ml^{-1} L-cysteine (Sigma), 0.3 mg ml^{-1} hyaluronidase (Sigma) and 100 U ml^{-1} DNAse (Sigma). After the enzymatic treatment the retina was transferred to a dish with cold Tyrode solution and washed twice before dissociation. Rods were mechanically dissociated by several serial passages through the tip of a wide bore plastic pipette. In the large majority of isolated rods, the axon and synaptic terminal were lost during the dissociation steps. Preservation of intact synaptic terminals in rods isolated from rabbit retinas requires longer enzymatic treatment than that used in the present work; in most cases, however, increasing the duration of enzymatic treatment results in outer segment (OS) damage. Therefore, immunolocalisation and electrophysiological properties of the channels were mainly investigated in rods without synaptic terminals.

Northern and Western blot analysis

Northern blot analysis. A Northern blot with 2–4 µg poly(A)$^+$ RNA from rabbit retina and hippocampus was hybridised, at 65 °C, with a ^{32}P-labelled cDNA probe corresponding to rabbit 3′ end (380 bp long, including 175 nt of 3′-UTR). The filter was washed with 2 × SSC–0.5 % SDS (2 × 15 min at 65 °C), 1 × SSC–0.5 % SDS (1 × 15 min at 65 °C), 0.1 × SSC–0.5 % SDS (1 × 15 min at room temperature) and exposed to X-ray film at −80 °C with an intensifying screen for 10 days (where SSC is saline sodium citrate; Sambrok *et al.* 1989). Normalisation was performed with murine glyceraldehyde phosphate dehydrogenase (GAPDH). Filters were stripped between subsequent hybridisations by pouring boiling 0.5 % SDS on them.

Western blot analysis. For Western blot analysis with anti-HCN1 antibody, protein extracts of retina and hippocampus were separated by a 10 % SDS–PAGE and electroblotted onto nitrocellulose membranes (Schleicher & Schuell s.r.l., Italy). Blocking and antibody incubations were carried out in Blotto solution (50 mM Tris pH 7.4, 150 mM NaCl, 0.1 % Tween-20, 5 % powdered skimmed milk). Anti-HCN1 was used at a 1:500 dilution. The polyclonal anti-HCN1 antibody was raised in rabbit against a peptide (STLISRPHPTWGESLASIP) which included residues 819–837 in the C-terminal tail of rabbit HCN1. This antibody has been used previously to demonstrate the expression of HCN1 in cardiac sinoatrial node cells (Moroni *et al.* 2001).

Secondary anti-rabbit antibodies coupled to horseradish peroxidase (HRP) (Bio-Rad, Italy) were used at a 1:5000 dilution and the bands visualised by incubation in ECL Western blotting detection reagents (Amersham Biosciences Italia, Italy).

Immunocytochemistry and confocal microscopy

For immunofluorescence, rabbit rod photoreceptors cells were isolated by enzymatic digestion and plated onto concanavalin A- (Boeheringer Ingelheim Italia S.p.a., Italy) coated coverslips (0.1 mg ml^{-1}) and let settle and stick for about 30 min. The cells were then fixed (5′ at 4 °C in either 0.5 % paraformaldehyde or absolute ethanol as indicated), quenched (0.1 M glycine in phosphate-buffered saline (PBS)), blocked (1 % bovine serum albumin (BSA), 0.4 % Saponin in PBS) and exposed either to anti-HCN1 antibody diluted 1:100 in blocking solution (treated) or preimmune serum (control). After washing in blocking solution, both control and treated cells were incubated with an appropriate dilution of fluorescein isothiocyanate (FITC)-conjugated secondary antibodies (Jackson Immunoresearch Laboratories, PA, USA). The samples were mounted with Mount Quick mounting medium (Bioptica, Italy). Images were collected with an inverted microscope (Nikon Eclipse TE300, Nikon Instruments S.p.a., Italy) equipped with a laser confocal scanning system (Radiance Plus, Bio-Rad) and a × 60 oil immersion objective. The acquisition software provided an additional magnification factor, ranging from 5 to 8. Fluorescence images were collected using the 488 nm excitation wavelength from an argon laser (Bio-Rad). Emitted light was filtered with 515–530 nm band-pass or 500 nm long-pass filters. Analysis of the fluorescent signal was performed with Scion image software (Scion Corporation, MD, USA).

Electrophysiology and data analysis

Electrophysiological recording of h-current in HEK 293 cells expressing homomeric rbHCN1 were carried out as previously reported (Moroni *et al.* 2001). Perforated-patch measurements were carried out at room temperature in rabbit rods isolated by enzymatic treatment, using the same methods as described for guinea-pig rods (Demontis *et al.* 1999). Perforated-patch recordings had series resistances up to 60 MΩ. In order to prevent oscillations, the series resistance was only partially compensated (50 %). In most cases, for current intensities up to −100 pA, generated in response to a 75 mV hyperpolarising step from −35 to −110 mV, the error associated with this partial compensation has an upper limit of 3 mV, that is less than 5 %. No correction was applied for this small error in the steady-state voltage. Partial compensation of the series resistance may nevertheless affect the settling time of the voltage clamp. However, considering a

capacitance of 2–6 pF for rods, the settling time of the voltage clamp ranges from 600 to 2100 μs (time constants ranging from 120 to 350 μs). Therefore the series resistance is not expected to affect the kinetics of voltage-dependent currents, which in rods activate with time constants exceeding 40 ms at room temperature (see Results).

In Fig. 3, in order to compare the voltage dependence of activation between I_h in rods and HCN1 expressed in HEK cells, hyperpolarisation-activated currents were recorded in the presence of 1 mM Ba^{2+} to block other voltage-dependent currents. Tail current amplitudes were measured at −60 mV, following a 2 s activating voltage step to a variable voltage in the range −110 to −20 mV. This duration was sufficient for steady-state activation to be reached at all voltages. Tail amplitudes were normalised, plotted as a function of the activating voltage and the resulting fractional activation parameter $y_\infty(V)$ was fitted to a Boltzmann equation:

$$y_\infty(V) = \frac{1}{1 + \exp\left(\dfrac{V - V_{\frac{1}{2}}}{s}\right)}, \quad (1)$$

where $V_{\frac{1}{2}}$ and s are the half-activation voltage and the inverse slope factor, respectively.

The tails method is standard for measurement of the activation curve of hyperpolarisation-activated currents (see for example DiFrancesco *et al.* 1986), being leak independent, since tail amplitudes are all measured upon deactivation at a fixed potential. Tail current analysis, on the other hand, is less adequate to analyse activation when two currents operate with minimal superposition of their activation ranges. In Fig. 4, in order to evaluate the effects of 8-Br-cAMP on rod voltage-dependent conductances, which include I_h and an ether-à-go-go-like K^+ current (I_{Kx}) (Beech & Barnes, 1989; Frings *et al.* 1998), we assumed that the total ionic current $I(V)$ through rod membranes is composed of three components: the current I_h, I_{Kx} and a leakage current (I_L). The steady-state I–V relation was therefore better described by the following equation, rather than by tail current analysis:

$$I(V) = \frac{G_h(V - E_h)}{1 + \exp\left(\dfrac{V - V_{\frac{1}{2}h}}{s_h}\right)} + \frac{G_{kx}(V - E_{Kx})}{1 + \exp\left(\dfrac{V - V_{\frac{1}{2}Kx}}{s_{Kx}}\right)} + G_L(V - E_L), \quad (2)$$

where G_h, G_{Kx} and G_L are the fully activated conductances; E_h, E_{Kx} and E_L the reversal potentials of I_h, I_{Kx} and I_L, respectively; and $V_{\frac{1}{2}h}$, $V_{\frac{1}{2}Kx}$ are the half-activation voltages and s_h s_{Kx} the inverse slope factors of I_h and I_{Kx}. This equation has previously been used to fit the I–V relation of guinea-pig rods (Demontis *et al.* 1999). In Fig. 4*C*, analysis by eqn (1) of tail currents measured at −70 mV provided estimates for $V_{\frac{1}{2}h}$ and its modification by cAMP that were in close agreement with those provided by fitting eqn (2) to the steady-state I–V data. We have included tail current analysis in Fig. 4*B* in order to allow a direct comparison between our data and those in the literature.

In describing the voltage dependence of I_h kinetics of activation in rods we have used $t_{\frac{1}{2}}$ (time required to reach 50 % activation of the current). In the past, activation kinetics of hyperpolarisation-activated currents have been described by single exponentials, by the sum of two independent single exponentials and by the square of single exponentials (DiFrancesco, 1984), aiming at reproducing aspects of the current gating that could not be accounted for by

Hodgkin–Huxley kinetic models. However, considering the lack of correspondence between these descriptions and a specific model of HCN kinetics, in describing the time course of hyperpolarisation-activated current activation we have preferred to adopt $t_{\frac{1}{2}}$. The use of $t_{\frac{1}{2}}$, which has recently been used by others to describe the effect of cAMP on the activation kinetics of HCN channels (Wainger *et al.* 2001), may therefore facilitate comparison with recent data.

To this end, leak currents were digitally subtracted off-line and $t_{\frac{1}{2}}$ was the time required to reach 50 % of the steady-state current, taking the rising phase of the current as time zero.

All values are reported as means ± S.E.M.

RESULTS

The results leading to identification of the HCN1 isoform in the rabbit retina are illustrated in Fig. 1. Northern blot analysis using an HCN1-specific probe identifies a band of appropriate size for HCN1 mRNA (9.1 kb) in both the retina (R) and the hippocampus (H) of rabbit (Fig. 1*A*).

The Western blot analysis in Fig. 1*B* was performed using an anti-HCN1 specific antibody, and yielded a prominent band of 105 kDa for the retina of rabbit. Differences in molecular mass of native HCN1 proteins between retina and hippocampus, as shown in Fig. 1*C*, may reflect differences in glycosylation, as originally reported for cloned HCN1 (Santoro *et al.* 1997).

In view of the recent report of selective expression of HCN1 mRNA in retinal rods (Moosmang *et al.* 2001), we have investigated the presence and the subcellular
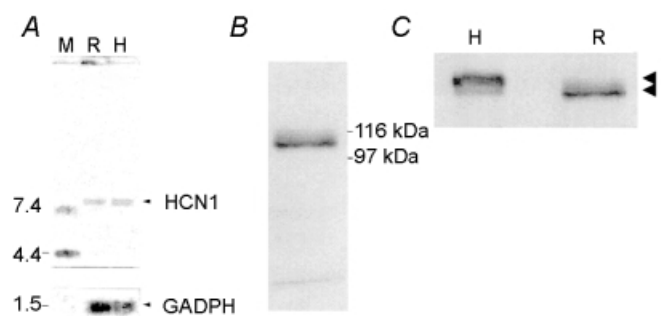

Figure 1. Northern and Western blot analysis of HCN1 expression in different rabbit tissues

A, Northern blot analysis of HCN1 mRNA expression in different rabbit tissues. Two micrograms of poly(A)$^+$ RNA, isolated from retina (R) and hippocampus (H) was loaded. The filter was probed with a DNA fragment of 380 bp in the 3′-UTR of rbHCN1. The position of molecular mass standards (M) is shown on the left. GAPDH (glyceraldehyde-3-phosphate dehydrogenase) was used as an internal control to check the quantity and integrity of loaded RNA. *B*, Western blot analysis of HCN1 protein in rabbit retina showing a prominent band of the calculated molecular mass of 105 kDa. *C*, Western blot comparative analysis of HCN1 in retina (R) and hippocampus (H). Arrowheads indicate the position of the prominent band in each tissue; 120 kDa in H and 105 kDa in R (calculated molecular mass). Thirty micrograms of protein was loaded per strip, and probed with anti-rbHCN1.

localisation of HCN1 in rabbit rods by immuno-cytochemistry, and the results are shown in Fig. 2.

In Fig. 2*A* and *B*, Nomarski images of two isolated rabbit rods are shown after fixation. Brackets indicate the different cell compartments. The confocal image in *C* illustrates the localisation of HCN1 in the cell body nuclear region (N) and inner segment (IS). Data in *E* show that stepping the voltage from −35 to −110 mV activates an inward current (thin trace) in an isolated rabbit rod. The recording configuration is schematically represented above the records. Note that the current at −110 is fully blocked by 3 mM CsCl (thick trace); CsCl does not affect the inward relaxation at −50 mV, which results from the deactivation of I_{Kx}. In agreement with the absence of HCN1 labelling in the outer segment (OS), no I_h current was observed in patch clamp recordings from an isolated OS (Fig. 2*F*). Figure 2*D* illustrates a control experiment, in which the rod was not treated with the anti-HCN1 antibody before exposure to the secondary FITC-conjugated antibody. In the absence of the anti-HCN1 primary antibody the rod was not labelled. Qualitatively similar results were observed when isolated rods were fixed with ethanol; however, labelling had a spotty appearance

and a higher level of labelling was present in the OS than in paraformaldehyde-fixed rods (data not shown).

We next addressed the functional properties of I_h in retinal rods, by characterising its steady-state voltage dependence of activation and kinetics. In Fig. 3*A*, I_h traces recorded from a rabbit rod upon stepping from −30 mV to voltages in the range −110 to −20 mV are shown.

Average values of the normalised tail current amplitude, as measured during current deactivation upon return to −60 mV, are plotted as open circles in Fig. 3*B*. In eight cells the mean $V_{1/2}$ was −75.3 ± 0.2 mV, and the inverse slope in rabbit rods was 7.5 ± 0.2 mV. The fractional steady-state conductance for homomeric rbHCN1 channels expressed in HEK 293 cells, shown in Fig. 3*B* as filled circles, was similar to that of I_h in rods, with an average $V_{1/2}$ (4 cells) of −75.3 ± 0.3 mV, and an inverse slope of 8.2 ± 0.4 mV. Fitting the steady-state conductances computed from steady-state *I–V* curves with eqn (2) provided similar estimates.

The contribution of different HCN isoforms was also investigated by analysing the activation kinetics of I_h. The voltage dependence of the time required to activate 50 %
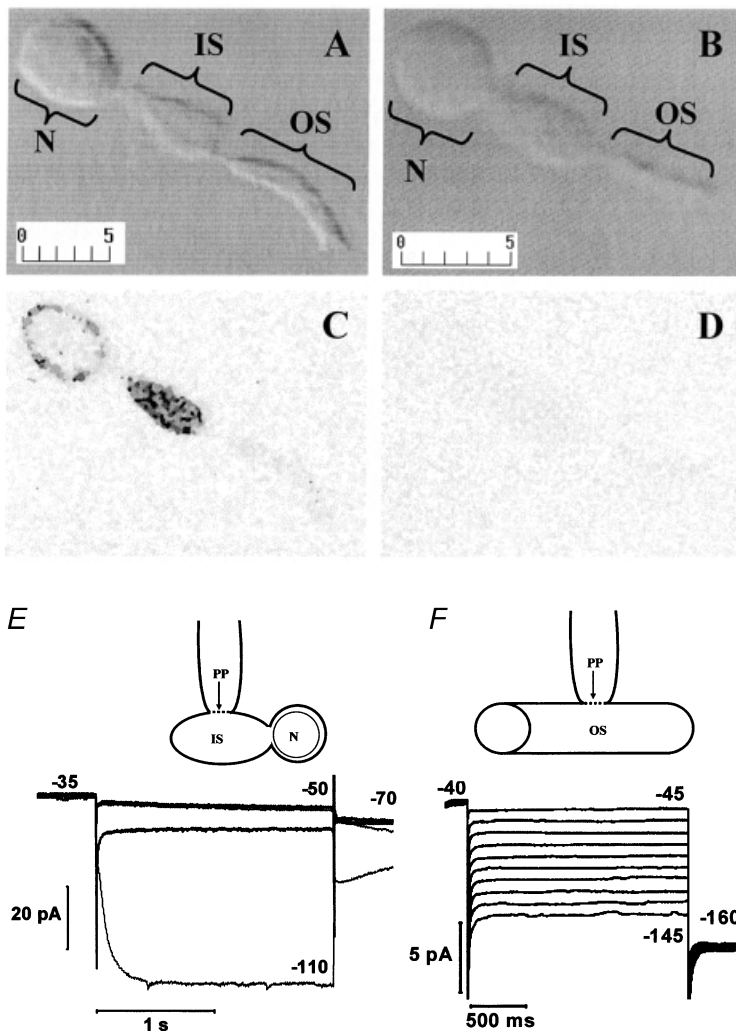

Figure 2. Immunolabelling of rabbit rod photoreceptors with anti-rbHCN1 antibody

A and *B*, Nomarski pictures of two para-formaldehyde-fixed isolated rabbit rods. The different functional compartments of the rod are indicated by brackets: OS, outer segment; IS, inner segment; N, cell body (nuclear) region. Calibration bars in micrometres are shown in the bottom left corner of each panel. *C* and *D*, greyscale images of rods in *A* and *B*, respectively, acquired using confocal fluorescence microscopy with identical laser energy and pinhole aperture. Anti-HCN1 antibody or preimmune serum was used in *C* and *D*, respectively, and the secondary anti-rabbit antibody was conjugated with fluorescein isothiocyanate (FITC). *E*, schematic drawing of the recording configuration from an isolated rod with intact IS and cell body and lacking OS and axon terminal. The arrow pointing to the plasma membrane contacted by the electrode indicates the perforated patch (PP). Traces at the bottom are perforated-patch recordings from an isolated rod with IS and cell body, as shown in the scheme above. Voltage steps of 2 s duration to −50 and −110 mV in control (thin trace) and in 3 mM CsCl (thick trace) were applied from a holding voltage of −35 mV. *F*, schematic drawing of the recording configuration from an isolated OS. Traces are perforated-patch clamp recordings from an isolated OS. The holding voltage was −40 mV. Voltage steps of 2 s duration ranged from −45 to −145 mV in 10 mV steps.

($t_{1/2}$) of I_h is illustrated in *C* for rabbit rods (open circles, $n = 8$), and is very similar to that of homomeric rbHCN1 channels expressed in HEK 293 cells (filled circles, $n = 4$).

These observations are consistent with the idea that homomeric HCN1 channels mediate I_h in rods.

We finally investigated the modulation of I_h by cAMP. As shown in Fig. 4*A*, 8-bromoadenosine 3′-5′-cyclic monophosphate (8-Br-cAMP), a membrane-permeant analogue of cAMP, increased the inward current at −80 and −110 mV. However, 8-Br-cAMP had no effect on the current amplitude and/or time course at −20 and −60 mV, which in the absence of Ba^{2+} mainly represents I_{Kx} deactivation.

This suggests that cAMP specifically affects I_h, without modifying either the leakage or the I_{Kx} current activated in the range −60 to −20 mV. This is confirmed by plotting the steady-state *I–V* relation in Fig. 4*B*, which shows that control (open circles) and cAMP (filled circles) currents are identical down to about −60 mV, but diverge at more negative voltages.

The continuous lines in Fig. 4*B* were best fits of measured values with eqn (2), and provide estimates for the effects of 8-Br-cAMP on the parameters describing the activation of voltage-dependent currents in rods. The action of 8-Br-cAMP on the I_h was to shift $V_{1/2h}$ by about 3 mV and to increase the maximum conductance (G_h) by about 11 % (from 883 to 979 pS). The G_h increase was consistently observed, and averaged 12 ± 2 %, a value significantly different from 0 ($P < 0.05$, paired *t* test, $n = 4$). The presence of a small 8-Br-cAMP-induced shift of $V_{1/2h}$ was confirmed by plotting the normalised amplitudes of I_h tail currents at −70 mV. As shown in Fig. 4*C* for four rods, 8-Br-cAMP (filled circles) shifted $V_{1/2}$ from -78.7 ± 0.3 mV in control (open circles) to -76.4 ± 0.4 mV in the presence of 200 μM 8-Br-cAMP (filled circles), with an average shift of 2.3 ± 0.8 mV ($P < 0.05$, paired *t* test, $n = 4$). In agreement with the shifting action on $V_{1/2h}$, 8-Br-cAMP also slightly accelerated the time course of I_h activation, as shown in the inset of Fig. 4*D*, where the −110 mV records in Fig. 4*A* are plotted on an expanded time scale after normalisation. In four rods, the time required to activate 50 % of the current ($t_{1/2}$) was reduced from 119 ± 7 ms in control to 97 ± 5 ms in 8-Br-cAMP ($P < 0.05$, two-way ANOVA), and the $t_{1/2}(V)$ relation in 8-Br-cAMP was shifted to less negative values by about 2.5 mV as compared to control values.

The functional significance of the modulation of I_h by cAMP was investigated by using 500 ms current steps of −2.5 and −10 pA, which approximate the dark current suppression induced by dim (−2.5 pA) and bright (−10 pA) flashes in mammalian rods (Baylor *et al.* 1984*b*; Tamura *et al.* 1989; Matthews, 1991). The data in Fig. 5 show that voltage responses in the presence of 200 μM

8-Br-cAMP (thick traces) are not significantly different from control records (thin traces). This result indicates that in the range of membrane potential of physiological relevance cAMP, does not affect the gain of current-to-voltage conversion in mammalian rods.
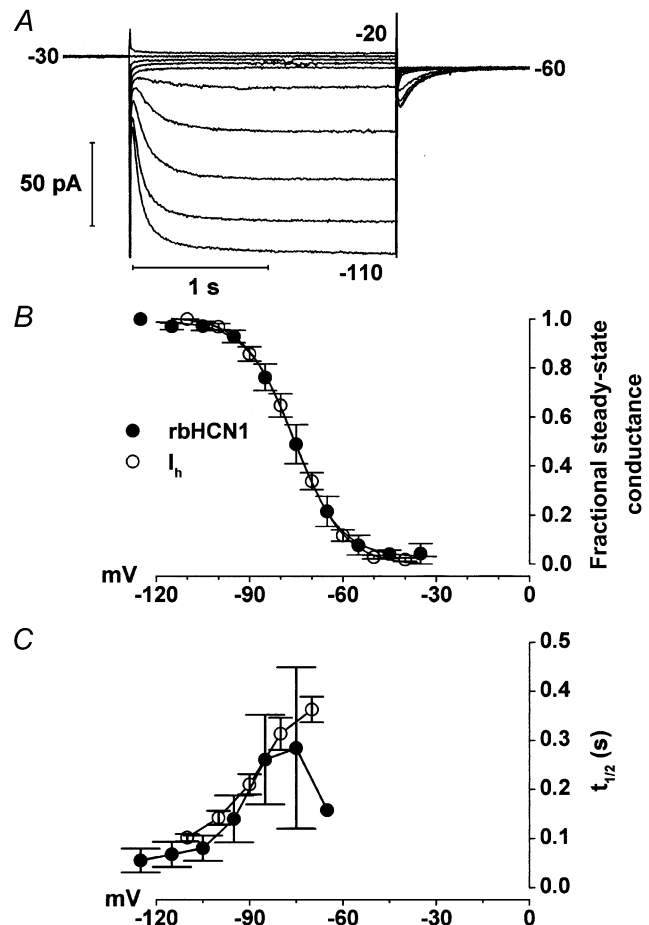

Figure 3. Properties of I_h in rabbit rod photoreceptors

A, currents activated in a rabbit rod by 2 s steps to voltages ranging from −20 to −110 mV in 10 mV steps. The holding voltage was −30 mV. Currents were recorded in the presence of 1 mM $BaCl_2$ to suppress the potassium current (I_{Kx}). *B*, activation curves for rabbit rod I_h and rbHCN1 current. Tail current amplitudes during protocols as in *A* were measured at −60 mV in 8 rods after the decay of capacitive transients, normalised to the maximum value, averaged and plotted against test voltage (steady-state fractional conductance; ○, mean ± S.E.M.). The thick line is the best fit of datapoints to eqn (1), which yielded $V_{1/2} = -75.3 \pm 0.2$ mV and $s = 7.5 \pm 0.2$ mV. ● are mean values (± S.E.M.) from $n = 4$ HEK 293 cells expressing homomeric rbHCN1. Data were obtained using a protocol previously described (Viscomi *et al.* 2001). The dotted trace is the best fit of datapoints to eqn (1), yielding $V_{1/2} = -75.3 \pm 0.3$ mV and $s = 8.2 \pm 0.4$ mV. *C*, voltage dependence of the time to half-activation ($t_{1/2}$) of rod I_h and rbHCN1 current. Points plotted are mean ± S.E.M. values from the 8 rods in *B* (○), and from the 4 cells in *B* that expressed homomeric rbHCN1 channels (●).

DISCUSSION

We have found that both HCN1 message and protein are expressed in the rabbit retina. Hyperpolarisation-activated currents have been demonstrated in monkey cones (Yagi & MacLeish, 1994) and in rat bipolar cells (Karschin & Wassle, 1990). A thorough investigation of the properties of I_h in cones and bipolar cell types was outside the scope of the present work, because the functional role of I_h in these cells is not well characterised as in rods. HCN1 protein was localised in rabbit rods by immunocytochemistry. Using perforated patch clamp analysis, we have shown in Fig. 3 that the kinetic properties of I_h in rabbit rods are similar to those of the heterologously expressed homomeric rbHCN1 current. Also, modulation of I_h by cAMP indicates a small shifting effect ($V_{1/2}$ shift of 2.3 mV), which is consistent with the limited action of cAMP on the kinetics of homomeric HCN1 channels. These immunocytochemical and functional data support the notion that the rod I_h is carried mainly through homomeric HCN1 channels. It is important to note that we did not look for other HCN isoforms, so that our data do not rule out the possibility that other HCN isoforms may be expressed in rods. However, our electrophysiological results suggest that

other HCN isoforms do not make a significant contribution to h-channels in rods.

The presence of I_h in guinea-pig rods (Demontis *et al.* 1999) and the expression of HCN1 mRNA in mouse rods (Moosmang *et al.* 2001) raise the possibility that the expression of HCN1 is a widespread feature among mammalian rods.

Localisation of HCN1 in rabbit rods

The confocal imaging of HCN1 shown in Fig. 2*A* indicates that the protein is not restricted to the surface membrane but is found in the cell interior as well. This distribution suggests that a substantial fraction of channel proteins stocks up in intracellular compartments such as the Golgi apparatus, to supply channel turnover.

Specific labelling by the HCN1 antibody was found at moderate to high levels in both the inner segment and the cell body. The localisation of voltage-dependent currents in the inner segment and/or cell body region has been previously proposed for amphibian rods on the grounds of electrophysiological measurements (Baylor *et al.* 1984*a*). Our data on the distribution of HCN1 in rabbit rods show that h-channels are strategically located in the proximal regions of the visual cell, IS and cell body, where the
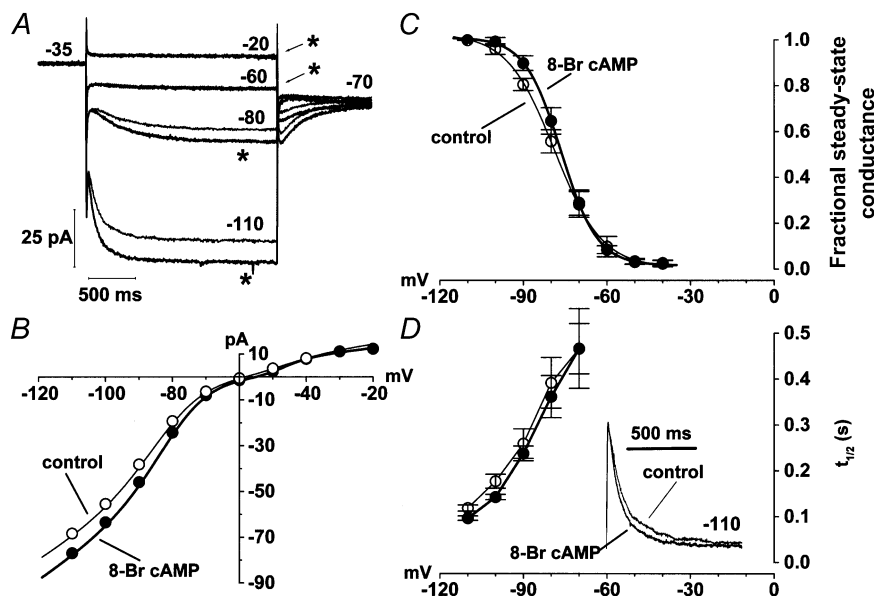

Figure 4. Effects of cAMP on I_h activation

A, currents activated by 2 s voltage steps at −110, −80, −60 and −20 mV, from a holding voltage of −35 mV, in control and in the presence of 200 μM 8-Br-cAMP (asterisks). *B*, current amplitudes measured at the end of 2 s activating steps as a function of voltage in control (○) and in the presence of 8-Br-cAMP (●). Lines are best fits to eqn (2). *C*, activation curves measured in $n = 4$ cells at −70 mV, in control condition (○) and in the presence of 8-Br-cAMP (●). Lines through symbols are best fits according to eqn (1), yielding $V_{1/2} = -78.7$ and −76.4 mV, and $s = 8.5$ and 6.5 mV for control and 8-Br-cAMP curves, respectively. *D*, voltage dependence of half-activation times ($t_{1/2}$; mean ± S.E.M.) in control (○) and in the presence of 8-Br-cAMP (●), as measured in $n = 4$ cells. Sweeps in the inset represent the time course of current activation for the records in *A* at −110 mV. The amplitude of the current recorded in 8-Br-cAMP was normalised to that of the control record. In order to measure the effect of cAMP on I_{Kx}, data in Fig. 4 were recorded in Tyrode solution, in the absence of Ba^{2+}.

photocurrent generated at the OS is converted into a voltage to be transmitted to second order neurones (see Demontis *et al.* 1999).

Modulation by cAMP of native HCN1 in rods

Data in Fig. 4 show that perfusion with 200 μM 8-Br-cAMP yields a small depolarising shift (about 3 mV) of the I_h activation curve and activation rate. This effect is slightly smaller than the 6.7 mV reported for homomeric rbHCN1 channels in whole-cell recordings from HEK 293 cells exposed to 100 μM phenyl-thio-cAMP, a membrane-permeant analogue of cAMP (Moroni *et al.* 2001). However, as already reported for homomeric HCN1 expressed in oocytes (Chen *et al.* 2001), I_h modulation by exogenous cAMP depends on the basal level of this cyclic nucleotide. The observation of a 5.6 mV shift for homomeric mHCN1 channels in inside-out macro-patches from HEK 293 cells exposed to cAMP (Viscomi *et al.* 2001) suggests that cAMP levels may be rather low in HEK 293 cells in our recording conditions. On the other hand, a high basal level of endogenous cAMP is consistent with the role of this second messenger in regulating melatonin production in mammalian rods (Cohen *et al.* 1992; Tosini & Dirden, 2000).

A possible explanation for the small shift of $V_{\frac{1}{2}h}$ in rods is that cAMP levels are high in light-adapted rods, so that the response to exogenously applied cAMP is occluded. This possibility seems unlikely because in mammals (Cohen *et al.* 1992) cAMP levels are higher in dark-adapted than in light-adapted rods. Furthermore, a hyperpolarising shift of I_h activation of about 3 mV (G. C. Demontis, unpublished observations) was observed in response to dopamine, which is known to inhibit cAMP accumulation in mammalian rods (Cohen *et al.* 1992). Although data are somewhat preliminary, the small shift observed with dopamine suggests that the basal level of endogenous cAMP in light-adapted rods may not occlude the response to 8-Br-cAMP.

Considering the functional role of cGMP in rods and the modulation of h-currents by both cAMP and cGMP (DiFrancesco & Tortora, 1991), it is tempting to speculate that endogenous cGMP may occlude the response to exogenous cAMP. However, in our recording conditions rods were exposed to bright light and the cGMP level was therefore low. Furthermore, cGMP is synthesised in the outer segment, where its diffusion is hindered (Koutalos *et al.* 1995). Considering the localisation of HCN1 in the inner segment (see Fig. 2), it is presently unclear whether cGMP may play a physiological role in the modulation of I_h by diffusing from the outer to the inner segment of rods.

Perfusion with 8-Br-cAMP also induces an increase in the maximal I_h current at full activation voltages (see Fig. 4*A*). A similar action is sometimes observed in HCN1 recordings (see for example Moroni *et al.* 2001).

Phosphatase inhibitors are known to increase total I_f in cardiac sinoatrial node cells (Accilli *et al.* 1997). However, the time course of this increase is slower than that of the shift in activation resulting from the direct modulation of I_f channels by cAMP (DiFrancesco & Tortora, 1991). Although we have not investigated this effect in detail, it is perhaps interesting to note that in rabbit rods the increase in total current and the shift of activation occur within the same time scale (< 2 min). Furthermore, a cAMP-dependent increase in total I_h has previously been reported to take place on a relatively rapid time scale in primary sensory (Ingram & Williams, 1996) and hippocampal neurones (Gasparini & DiFrancesco, 1999). In primary sensory neurones, both Rp and Sp cAMP are equally effective, suggesting that the increase in total I_h is phosporylation independent (Ingram & Williams, 1996). In this regard, recent results (Yu *et al.* 2001) suggest that HCN1 may associate with Mink-related peptide 1 (MiRP 1) (Abbott *et al.* 1999), to increase HCN1 expression and accelerate its activation kinetics.

Why do rods express voltage-dependent channels with a cyclic nucleotide binding site?

In the range of membrane potentials of physiological significance, two main currents control the *I–V* relation of vertebrate rods. The first is a barium-sensitive potassium current (I_{Kx}) (Beech & Barnes, 1989), which shapes the voltage generated in response to small currents, such as those generated by dim light stimuli (Owen & Torre, 1983). The second is a caesium-sensitive hyper-polarisation-activated current (I_h) (Bader & Bertrand, 1984), which shapes the response to bright stimuli (Fain *et al.* 1978; Schneeweis & Schnapf, 1999).
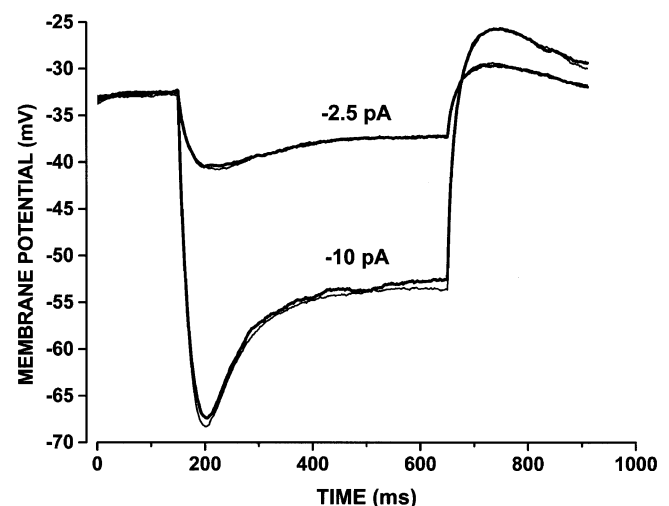

Figure 5. Effects of cAMP on the voltage response of rods

Voltage responses from a rabbit rod to 500 ms current steps of −2.5 and −10 pA, in control (thin traces) and in the presence of 200 μM 8-Br-cAMP (thick traces). The rod was recorded in Tyrode solution.

At the molecular level, two splice variants of the ether-à-go-go (eag) channels have been cloned from bovine retina and proposed to be part of the channels carrying I_{Kx} in rods (Frings *et al.* 1998). Eag and HCN channels are characterised by the six membrane-spanning domains typical of potassium channels and a cyclic nucleotide-binding domain. However, the mammalian eag channel lacks the cAMP sensitivity and calcium permeability of *Drosophila* eag, suggesting that I_{Kx} in mammalian rods may lack cAMP sensitivity (Frings *et al.* 1998). Our results, showing that the *I–V* relation and the voltage response of rabbit rods are not affected by cAMP in the range of membrane potentials that gate I_{Kx}, provides experimental support to this hypothesis.

The significance of current to voltage conversion in rods by two channels, both having a cyclic nucleotide binding domain, but fully lacking (I_{Kx}) or with moderate (I_h) sensitivity to cAMP, is puzzling. This may indicate that signal processing in rods has been designed for minimal interference from cAMP turnover. This hypothesis is consistent with the observation by Schneeweis & Schnapf (1999) that dopamine, a transmitter that modulates cAMP turnover in mammalian rods (Cohen *et al.* 1992), does not affect the rod component of the photoresponse in cones of monkey. However, see Akopian & Witkovsky (1996) for dopamine modulation of I_h in amphibian rods.

In this respect, selecting channels with low conductance (DiFrancesco, 1986; Zimmerman & Baylor, 1986), such as those with a cyclic nucleotide binding site in their carboxy-terminal, may help to minimise noise in the processing of small signals generated in rods by single photon absorption (see Bialek & Owen, 1990).

REFERENCES

ABBOTT, G. W., SESTI, F., SPLAWSKI, I., BUCK, M. E., LEHMANN, M. H., TIMOTHY, K. W., KEATING, M. T. & GOLDSTEIN, S. A. (1999). MiRP1 forms IKr potassium channels with HERG and is associated with cardiac arrhythmia. *Cell* **97**, 175–187.

ACCILLI, E. A., REDAELLI, G. & DIFRANCESCO, D. (1997). Differential control of the hyperpolarization-activated current (i_f) by cAMP gating and phosphatase inhibition in rabbit sino-atrial node myocytes. *Journal of Physiology* **500**, 643–651.

AKOPIAN, A. & WITKOVSKY, P. (1996). D2 dopamine receptor-mediated inhibition of a hyperpolarization-activated current in rod photoreceptors. *Journal of Neurophysiology* **76**, 1828–1835.

BADER, C. R. & BERTRAND, D. (1984). Effect of changes in intra- and extracellular sodium on the inward (anomalous) rectification in salamander photoreceptors. *Journal of Physiology* **347**, 611–631.

BAYLOR, D. A., MATTHEWS, G. & NUNN, B. J. (1984*a*). Location and function of voltage-sensitive conductances in retinal rods of the salamander *Ambystoma tigrinum*. *Journal of Physiology* **354**, 203–223.

BAYLOR, D. A., NUNN, B. J., & SCHNAPF, J. L. (1984*b*). The photocurrent, noise and spectral sensitivity of rods of the monkey *Macaca fascicularis*. *Journal of Physiology* **357**, 575–607.

BEECH, D. J. & BARNES, S. (1989). Characterisation of a voltage-gated K channels that accelerates the rod response to dim light. *Neuron* **3**, 573–581.

BIALEK, W. & OWEN, W. G. (1990). Temporal filtering in retinal bipolar cells. Elements of an optimal computation? *Biophysical Journal* **58**, 1227–1233.

CALVERT, P. D., GOVARDOVSKII, V. I., KRASNOPEROVA, N., ANDERSON, R. E., LEM, J. & MAKINO, C. L. (2001). Membrane protein diffusion sets the speed of rod phototransduction. *Nature* **411**, 90–94.

CHEN, S., WANG, J. & SIEGELBAUM, S. A. (2001). Properties of hyperpolarization-activated pacemaker current defined by coassembly of HCN1 and HCN2 subunits and basal modulation by cyclic nucleotide. *Journal of General Physiology* **117**, 491–504.

COHEN, A. I., TODD, R. D., HARMON, S. & O'MALLEY, K. (1992). Photoreceptors of mouse retinas possess D4 receptors coupled to adenylate cyclase. *Proceedings of the National Academy of Sciences of the USA* **89**, 12093–12097.

DEMONTIS, G. C., LONGONI, B., BARCARO, U. & CERVETTO, L. (1999). Properties and functional roles of hyperpolarization-gated currents in guinea-pig retinal rods. *Journal of Physiology* **515**, 813–828.

DIFRANCESCO, D. (1984). Characterization of the pace-maker current kinetics in calf Purkinje fibres. *Journal of Physiology* **348**, 341–367.

DIFRANCESCO, D. (1986). Characterisation of single pacemaker channels in cardiac sino-atrial node cells. *Nature* **324**, 470–473.

DIFRANCESCO, D. (1993). Pacemaker mechanisms in cardiac tissue. *Annual Review of Physiology* **55**, 455–472.

DIFRANCESCO, D. (1999). Dual allosteric modulation of pacemaker (f) channels by cAMP and voltage in rabbit SA node. *Journal of Physiology* **515**, 367–376.

DIFRANCESCO, D., FERRONI, A., MAZZANTI, M. & TROMBA, C. (1986). Properties of the hyperpolarizing-activated current (I_f) in cells isolated from the rabbit sino-atrial node. *Journal of Physiology* **377**, 61–88.

DIFRANCESCO, D. & TORTORA, P. (1991). Direct activation of cardiac pacemaker channels by intracellular cyclic AMP. *Nature* **351**, 145–147.

FAIN, G. L., QUANDT, F. N., BASTIAN, B. L. & GERSCHENFELD, H. M. (1978). Contribution of a caesium-sensitive conductance increase to the rod photoresponse. *Nature* **272,** 466–469.

FRANZ, O., LISS, B., NUE, A. & ROEPER, J. (2000). Single-cell mRNA expression of HCN1 correlates with a fast gating phenotype of hyperpolarization-activated cyclic nucleotide-gated channels (I_h) in central neurons. *European Journal of Neuroscience* **12**, 2685–2693.

FRINGS, S., BRULL, N., DZEJA, C., ANGELE, A., HAGEN, V., KAUPP, U. B. & BAUMANN, A. (1998). Characterization of ether-à-go-go channels present in photoreceptors reveals similarity to I_{kx}, a K$^+$ current in rod inner segments. *Journal of General Physiology* **111**, 583–599.

GARGINI, C., DEMONTIS, G. C., BISTI, S. & CERVETTO, L. (1999*b*). Effects of blocking the hyperpolarization-activated current (I_h) on the cat electroretinogram. *Vision Research* **39**, 1767–1774.

GARGINI, C., DEMONTIS, G. C., CERVETTO, L. & BISTI, S. (1999*a*). Analysis of pharmacologically isolated components of the ERG. *Vision Research* **39**, 1759–1766.

GASPARINI, S. & DIFRANCESCO, D. (1999). Action of serotonin on the hyperpolarization-activated cation current (I_h) in rat CA1 hippocampal neurons. *European Journal of Neuroscience* **11**, 3093–3100.

GAUSS, R., SEIFERT, R. & KAUPP, U. B. (1998). Molecular identification of a hyperpolarization-activated channel in sea urchin sperm. *Nature* **393**, 583–587.

INGRAM, S. L. & WILLIAMS, J. T. (1996). Modulation of the hyperpolarization-activated current (I_h) by cyclic nucleotides in guinea-pig primary afferent neurons. *Journal of Physiology* **492**, 97–106.

KARSCHIN, A. & WASSLE, H. (1990). Voltage- and transmitter-gated currents in isolated rod bipolar cells of rat retina. *Journal of Neurophysiology* **63**, 860–876.

KOUTALOS, Y., NAKATANI, K. & YAU, K. W. (1995). Cyclic GMP diffusion coefficient in rod photoreceptor outer segments. *Biophysical Journal* **68**, 373–382.

LUDWIG, A., ZONG, X., JEGLITSCH, M., HOFMANN, F. & BIEL, M. (1998). A family of hyperpolarization-activated mammalian cation channels. *Nature* **393**, 587–591.

LUDWIG, A., ZONG, X., STIEBER, J., HULLIN, R., HOFFMAN, F. & BIEL, M. (1999). Two pacemaker channels from human heart with profoundly different activation kinetics. *EMBO Journal* **18**, 2323–2329.

MATTHEWS, H. R. (1991). Incorporation of chelator into guinea-pig rods shows that calcium mediates mammalian photoreceptor light adaptation. *Journal of Physiology* **436**, 93–105

MOOSMANG, S., BIEL, M., HOFMANN, F. & LUDWIG, A. (1999). Differential distribution of four hyperpolarization-activated cation channels in mouse brain. *Biological Chemistry* **380**, 975–980.

MOOSMANG, S., STIEBER, J., ZONG, X., BIEL, M., HOFMANN, F. & LUDWIG, A. (2001). Cellular expression and functional characterization of four hyperpolarization-activated pacemaker channels in cardiac and neuronal tissues. *European Journal of Biochemistry* **268**, 1646–1652.

MORONI, A., BARBUTI, A., ALTOMARE, C., VISCOMI, C., MORGAN, J., BARUSCOTTI, M. & DIFRANCESCO, D. (2000). Kinetic and ionic properties of the human HCN2 pacemaker channel. *Pflügers Archiv* **439,** 618–626.

MORONI, A., GORZA, L., BELTRAME, M., GRAVANTE, B., VACCARI, T., BIANCHI, M. E., ALTOMARE, C., LONGHI, R., HEURTEAUX, C., VITADELLO, M., MALGAROLI, A. & DIFRANCESCO, D. (2001). Hyperpolarization-activated cyclic nucleotide-gated channel 1 is a molecular determinant of the cardiac pacemaker current I_f. *Journal of Biological Chemistry* **276**, 29233–29241.

MULLER, F., SCHOLTEN, A., IVANOVA, E., HAVERKAMP, S., KREMMER, E., GRUNERT, U. & KAUPP, B. (2001). HCN channels in the mammalian retina. *Society for Neuroscience Abstracts* **27**, 284.6

OWEN, G. W. & TORRE, V. (1983). High-pass filtering of small signals by retinal rods. Ionic studies. *Biophysical Journal* **41**, 325–339.

PAPE, H. C. (1996). Queer current and pacemaker: the hyperpolarization-activated cation current in neurons. *Annual Review of Physiology* **58**, 299–327.

SAMBROOK, J., FRITSCH, E. F. & MANIATIS, T. (1989) In *Molecular Cloning. A laboratory manual*, 2nd edn. Cold Spring Harbor Laboratory Press.

SANTORO, B., CHEN, S., LUTHI, A., PAVLIDIS, P., SHUMYATSKY, G. P., TIBBS, G. R. & SIEGELBAUM, S. A. (2000). Molecular and functional heterogeneity of hyperpolarization-activated pacemaker channels in the mouse CNS. *Journal of Neuroscience* **20**, 5264–5275.

SANTORO, B., GRANT, S. G., BARTSCH, D. & KANDEL, E. R. (1997). Interactive cloning with the SH3 domain of N-src identifies a new brain specific ion channel protein, with homology to eag and cyclic nucleotide-gated channels. *Proceedings of the National Academy of Sciences of the USA* **94**, 14815–14820.

SANTORO, B., LIU, D. T., YAO, H., BARTSCH, D., KANDEL, E. R., SIEGELBAUM, S. A. & TIBBS G. R. (1998). Identification of a gene encoding a hyperpolarization-activated pacemaker channel of brain. *Cell* **93**, 717–729.

SCHNEEWEIS, D. M. & SCHNAPF, J. L. (1999). The photovoltage of macaque cone photoreceptors: adaptation, noise, and kinetics. *Journal of Neuroscience* **19**, 1203–1216.

SEIFERT, R., SCHOLTEN, A., GAUSS, R., MINCHEVA, A., LICHTER, P. & KAUPP, U. B. (1999). Molecular characterization of a slowly gating human hyperpolarization-activated channel predominantly expressed in thalamus, heart, and testis. *Proceedings of the National Academy of Sciences of the USA* **96**, 9391–9396.

TAMURA, T., NAKATANI, K. & YAU, K. W. (1989). Light adaptation in cat retinal rods. *Science* **245**, 755–758.

TOSINI, L. & DIRDEN, J. C. (2000). Dopamine inhibits melatonin release in the mammalian retina: *in vitro* evidence. *Neuroscience Letters* **286**, 119–122

ULENS, C. & TYTGAT, J. (2001). Functional heteromerization of HCN1 and HCN2 pacemaker channels. *Journal of Biological Chemistry* **276**, 6069–6072.

VISCOMI, C., ALTOMARE, C., BUCCHI, A., CAMATINI, E., BARUSCOTTI, M., MORONI, A. & DIFRANCESCO, D. (2001). *Journal of Biological Chemistry* **276**, 29930–29934.

WAINGER, B. J., DEGENNARO, M., SANTORO, B., SIEGELBAUM, S. A. & TIBBS, G. R. (2001). Molecular mechanism of cAMP modulation of HCN pacemaker channels. *Nature* **411**, 805–810.

YAGI, T. & MACLEISH, P. R. (1994). Ionic conductances of monkey solitary cone inner segments. *Journal of Neurophysiology* **71**, 656–665.

YU, H., WU, J., POTAPOVA, I., WYMORE, R. T., HOLMES, B., ZUCKERMAN, J., PAN, Z., WANG, H., SHI, W., ROBINSON, R. B., EL-MAGHRABI, M. R., BENJAMIN, W., DIXON, J., MCKINNON, D., COHEN, I. S. & WYMORE, R. (2001). MinK-related peptide 1: A beta subunit for the HCN ion channel subunit family enhances expression and speeds activation. *Circulation Research* **88**, E84–87.

ZIMMERMAN, A. L. & BAYLOR, D. A. (1986). Cyclic GMP-sensitive conductance of retinal rods consists of aqueous pores. *Nature* **321**, 70–72.

Water Transport Controversies Special Issue

The Journal of Physiology